Medical Image Analysis 20 (2015) 52–60

Contents lists available at ScienceDirect

Medical Image Analysis

journal homepage: www.elsevier.com/locate/media

Manifold learning on brain functional networks in aging

Anqi Qiu [a,b,c,*], Annie Lee [a], Mingzhen Tan [a], Moo K. Chung [d,e]

[a] Department of Biomedical Engineering, National University of Singapore, Singapore
[b] Singapore Institute for Clinical Sciences, Agency for Science, Technology and Research, Singapore
[c] Clinical Imaging Research Center, National University of Singapore, Singapore
[d] Waisman Laboratory for Brain Imaging and Behavior, University of Wisconsin-Madison, USA
[e] Department of Biostatistics and Medical Informatics, University of Wisconsin-Madison, USA

ARTICLE INFO

Article history:
Received 11 October 2013
Received in revised form 5 August 2014
Accepted 21 October 2014
Available online 30 October 2014

Keywords:
Resting state fMRI
Symmetric positive definite matrix
Log-Euclidean Riemannian manifold
Locally linear embedding
Ridge regression

ABSTRACT

We propose a new analysis framework to utilize the full information of brain functional networks for computing the mean of a set of brain functional networks and embedding brain functional networks into a low-dimensional space in which traditional regression and classification analyses can be easily employed. For this, we first represent the brain functional network by a symmetric positive matrix computed using sparse inverse covariance estimation. We then impose a Log-Euclidean Riemannian manifold structure on brain functional networks whose norm gives a convenient and practical way to define a mean. Finally, based on the fact that the computation of linear operations can be done in the tangent space of this Riemannian manifold, we adopt Locally Linear Embedding (LLE) to the Log-Euclidean Riemannian manifold space in order to embed the brain functional networks into a low-dimensional space. We show that the integration of the Log-Euclidean manifold with LLE provides more efficient and succinct representation of the functional network and facilitates regression analysis, such as ridge regression, on the brain functional network to more accurately predict age when compared to that of the Euclidean space of functional networks with LLE. Interestingly, using the Log-Euclidean analysis framework, we demonstrate the integration and segregation of cortical–subcortical networks as well as among the salience, executive, and emotional networks across lifespan.

1. Introduction

The brain at rest is not idle but shows continuous, spontaneous fluctuations in activity among spatially distributed but functionally connected regions. Resting state functional magnetic resonance imaging (rs-fMRI) has been recognized as a useful technique to investigate complex patterns of brain functional organization at rest. It has been increasingly used in studies of normal aging and neurodegenerative diseases (Venkataraman et al., 2013; Deligianni et al., 2011; Bluhm et al., 2008; Wang et al., 2010; Tomasi and Volkow, 2012) as it is unbiased to confounds associated with task-based fMRI, such as task difficulty and performance.

A large body of rs-fMRI aging studies have employed graph theory to characterize "small-world" properties of the brain across lifespan, meaning that many networks have both local clustering of connections and a short path length between any two brain regions (Achard and Bullmore, 2007; Bullmore and Sporns, 2012; Meunier et al., 2009). However, a decrease of both global and local network efficiency was shown in older adults in comparison to young adults (Achard and Bullmore, 2007). Using graph theory, Newman's modularity metric can be defined to measure the strength of division of the brain functional network into modules. Previous studies (e.g., (Meunier et al., 2009)) revealed that normal brain aging was associated with changes in modularity of sparse functional networks. In particular, both young and older brain networks demonstrated significantly non-random modularity but the older brain showed a reduced number of intermodular connections to frontal modular regions and an increased number of connector nodes in posterior and central modules (Meunier et al., 2009). In addition to the aforementioned metrics that characterize the topology of the brain functional network, researchers also investigated age-related effects on the connectivity of individual structures and showed the age decline of major functional connectivity hubs in the 'default-mode' network (DMN) (Damoiseaux et al., 2008a; Bluhm et al., 2008; Wang et al., 2010; Tomasi and Volkow, 2012). A reduction of the connectivity between the anterior cingulate cortex and bilateral insular in salience network in older adults

* Corresponding author at: Department of Biomedical Engineering, National University of Singapore, 9 Engineering Drive 1, Block EA 03-12, Singapore 117576, Singapore. Tel.: +65 6516 7002; fax: +65 6872 3069.

E-mail address: bieqa@nus.edu.sg (A. Qiu).

http://dx.doi.org/10.1016/j.media.2014.10.006
1361-8415/

suggested an age-related deficits in decision-making and sensory integration (Onoda et al., 2012; Seeley et al., 2007). Decreased functional connectivity in the left premotor area and right cingulate motor cortex was found in older adults in comparison to young adults (Wu et al., 2007).

Recently, support vector machine (SVM) has been employed on rs-fMRI for the prediction of individual brain maturity, in which a subset of elements in the functional connectivity matrix derived from rs-fMRI were used as features (Dosenbach et al., 2010). Wang et al. (2012) assumed that variations of the functional networks are driven by variations in a small subset of unknown parameters. A supervised locality preserving projection (LPP) algorithm (He et al., 2005) was employed to learn a low-dimensional representation of brain development from many individuals at different ages and support vector regression (SVR) models were designed in this low-dimensional space for making continuously valued predictions about the functional development levels of individual brains. However, arithmetic operations on the matrices of brain functional networks, such as non-convex Euclidean operations, could result in undesirable properties of the matrices as discussed below.

Brain function network modeling has thus far largely based on (partial) correlation analysis of rs-fMRI time series data among brain regions, suggesting that the brain functional network can be fully characterized by a symmetric positive semi-definite matrix. Ideally, if the brain parcellated regions, served as network nodes, are functionally distinct from each other, then the functional network can be represented by a symmetric positive definite (SPD) matrix. When considering a SPD matrix as an element in a finite-dimensional Euclidean space, arithmetic operations, such as mean, does not satisfy certain desirable properties. For example, the linear average of SPD matrices is not the inverse of the linear average of the inverses of the SPD matrices. There have been great efforts on carrying out computations with SPD matrices in a curved space, called a manifold, in medical image analysis (Fillard et al., 2007; Arsigny et al., 2006; Pennec et al., 2006). In the manifold setting, a SPD matrix can be represented as an element in a vector space in which the mean and variance of SPD matrices can be easily computed with certain desirable properties. For instance, Arsigny et al. (2007) proposed a Riemannian framework on SPD matrices, which leads to the computation of the mean of SPD matrices while preserving the aforementioned desirable properties. It has been widely used to study the mean and variation of diffusion tensor imaging of the brain (Fillard et al., 2007). This manifold setting of SPD has been recently employed to investigate brain functional-connectivity difference in post-stroke patients (Varoquaux et al., 2010), which demonstrates an increase in statistical power in detecting functional disconnections in the patients when compared to the Euclidean setting of SPD. Manifold learning analysis was also widely used for studying anatomical shapes (e.g. (Aljabar et al., 2011)).

Here, we adopt the Riemannian framework of SPD matrices introduced by Arsigny et al. (2007) and propose a new analysis framework to utilize the full information of brain functional networks for computing the mean of a set of brain functional networks and embedding brain functional networks into a low-dimensional space in which regression and classification analyses can be easily employed. For this, we first represent the brain functional network by a SPD matrix computed using sparse inverse covariance estimation (Huang et al., 2010). Huang et al. (2010) employed the sparse inverse covariance estimation approach to compute functional connectivity matrices at different sparsity levels and detected differences of functional connectivity among mild cognitive impairment patients, Alzheimer's patients and normal controls. We then impose a Log-Euclidean Riemannian manifold structure on brain functional networks whose norm gives a convenient and practical way to define a mean. The metric in the Log-Euclidean Riemannian manifold leads to easy and efficient computation of the mean of SPD matrices. This is different from the work in Varoquaux et al. (2010), where affine-invariant metric in the Riemannian manifold of SPD matrices is used and involves intensive computation of matrix inverses, square roots, logarithms, and exponentials. Varoquaux et al. (2010) proposed a matrix variate probabilistic model suitable for inter-subject comparison of functional connectivity matrices on the affine-invariant manifold of SPD matrices, leading to a new algorithm for principled comparison of connectivity coefficients between pairs of regions. Finally, based on the fact that the computation of linear operations can be done in the tangent space of this Riemannian manifold, we adopt Locally Linear Embedding (LLE) (Roweis and Saul, 2000) to the Log-Euclidean Riemannian manifold space for embedding the brain functional networks into a low-dimensional space. Using this framework, we show the evolution of the brain functional network across lifespan and the comparison between the Log-Euclidean and Euclidean spaces of brain functional networks in terms of the prediction accuracy of biological age.

2. Methods

2.1. Subjects

This study was approved by the National University of Singapore Institutional Review Board. All participants provided written informed consent prior to the participation. Two-hundreds and fourteen healthy Singaporean Chinese volunteers aged 21–80 years old were recruited (males: 93; females: 121) for this study. The participants were recruited via advertisements and screened for eligibility through a phone interview prior to an onsite visit. Volunteers with the following conditions were excluded: (1) major illnesses/surgery (heart, brain, kidney, lung surgery); (2) neurological or psychiatric disorders; (3) learning disability or attention deficit; (4) head injury with loss of consciousness; (5) non-removable metal objects on/in the body such as cardiac pacemaker; (8) diabetes or obesity; (9) a Mini-Mental State Examination (MMSE) score of less than 24 (Ng et al., 2007). This study only included 178 right-handed subjects (age: 22–79 years; males: 71; females: 107) who completed structural and function MRI. The distribution of age among these subjects is shown in Fig. 1.

2.2. MRI acquisition and analysis

MRI was performed on a 3T Siemens Magnetom Trio Tim scanner using a 32-channel head coil at Clinical Imaging Research Centre of the National University of Singapore. The image protocols

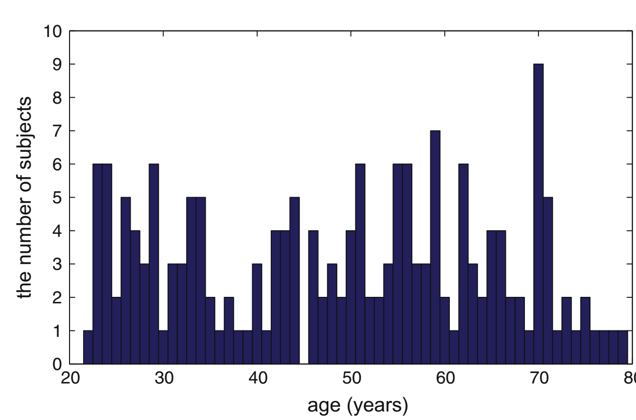

Fig. 1. Age distribution among 178 subjects.

were: (i) high-resolution isotropic T_1-weighted Magnetization Prepared Rapid Gradient Recalled Echo (MPRAGE; 192 slices, 1 mm thickness, in-plane resolution 1 mm, no inter-slice gap, sagittal acquisition, field of view 256 × 256 mm, matrix = 256 × 256, repetition time = 2300 ms, echo time = 1.90 ms, inversion time = 900 ms, flip angle = 9°); (ii) isotropic axial rs-fMRI imaging protocol (single-shot echo-planar imaging; 48 slices with 3 mm slice thickness, no inter-slice gaps, matrix = 64 × 64, field of view = 192 × 192 mm, repetition time = 2300 ms, echo time = 25 ms, flip angle = 90°, scanning time = 8.01 min); The subjects were asked to close their eyes during the rs-fMRI scan. The image quality was verified immediately after the acquisition through visual inspection when adults were still in the scanner. If the motion artifact was large, a repeated scan was conducted. The image was removed from the study if no acceptable image was acquired after three repetitions.

For the T_1-weighted image, FreeSurfer was used to segment the cortical and subcortical regions and the cortical parcellation. Briefly, a Markov random field (MRF) model was used to label each voxel in the T_1-weighted image as gray matter (GM), or white matter (WM), or CSF, or subcortical structures (hippocampus, amygdala, caudate, putamen, globus pallidus, and thalamus) (Fischl et al., 2002). Cortical inner surface was constructed at the boundary between GM and WM and then propagated to its outer surface at the boundary between GM and CSF. The cortical surface of each hemisphere was parcellated in 34 cortical regions (see panel of the cortical parcellation in Fig. 2) (Fischl et al., 2004) that will be used along with the 6 subcortical regions as ROIs in the resting-state fMRI analyses below.

The resting-state fMRI data were first processed with slice timing, motion correction, skull stripping, band-pass filtering (0.01–0.08 Hz) and grand mean scaling of the data (to whole brain modal value of 100). To quantify the quality of rs-fMRI data in terms of head motion, displacement due to motion averaged over the image volume was calculated for individual subjects. Its mean and standard deviation were respectively 0.05 mm and 0.04 mm among all the subjects used in this study. The resting-state fMRI signals due to effects of nuisance variables, including six parameters obtained by motion correction, ventricular and white matter signals were removed. Subsequently, the fMRI data were transferred to the corresponding T_1-weighted image via affine transformation and were finally represented on the cortical surface (see details in (Qiu et al., 2006)). For the functional network analysis, the functional time series in the ROIs defined above were first computed by averaging the signal of all voxels within individual ROIs. The functional connectivity of each subject was then characterized using an 80 × 80 symmetric matrix whose element *ij* was computed using Pearson correlation analysis on the time series of regions *i* and *j*.

2.3. Positive definite matrices for the representation of brain functional networks

As described above, the brain functional network is represented by a correlation matrix, R, where the ijth element of R is computed as the Pearson correlation coefficient of functional time series data, $f_i(t)$ and $f_j(t)$, over different time points in the ith and jth regions of interest (ROIs). From this construction, R is a symmetric matrix but is not necessarily a positive definite matrix partially due to unknown parcellation that divides the brain into distinct functional regions. More importantly, the estimation of R is in general achieved by maximum likelihood estimation (MLE) of the covariance matrix when $f_i(t)$ is mean centered and normalized with standard deviation of one. The log-likelihood can be written as

$$\begin{aligned} L(R^{-1}) &= \log\det R^{-1} - \frac{1}{n}\sum_{i=1}^{n} \mathbf{f}(t_j)^{\top} R^{-1} \mathbf{f}(t_j) \\ &= \log\det R^{-1} - \mathrm{trace}(R^{-1}S), \end{aligned} \quad (1)$$

where $S = \frac{1}{n}\sum_{j=1}^{n} \mathbf{f}(t_j)\mathbf{f}(t_j)^{\top}$ is the covariance matrix of

$$\mathbf{f}(t_j) = [f_1(t_j), \ldots, f_i(t_j), \ldots, f_p(t_j)]^{\top},$$

a vector containing functional values at time t_j for individual brain regions, i. n is the number of time points in the functional data. Based on our image acquisition protocol, $n = 206$. p denotes the number of brain regions. In our case, $p = 80$. Here, the log-likelihood is characterized as a function of R^{-1} to simply emphasize the estimation of the inverse covariance matrix. A limitation of MLE is that the estimated covariance matrix is positive definite only

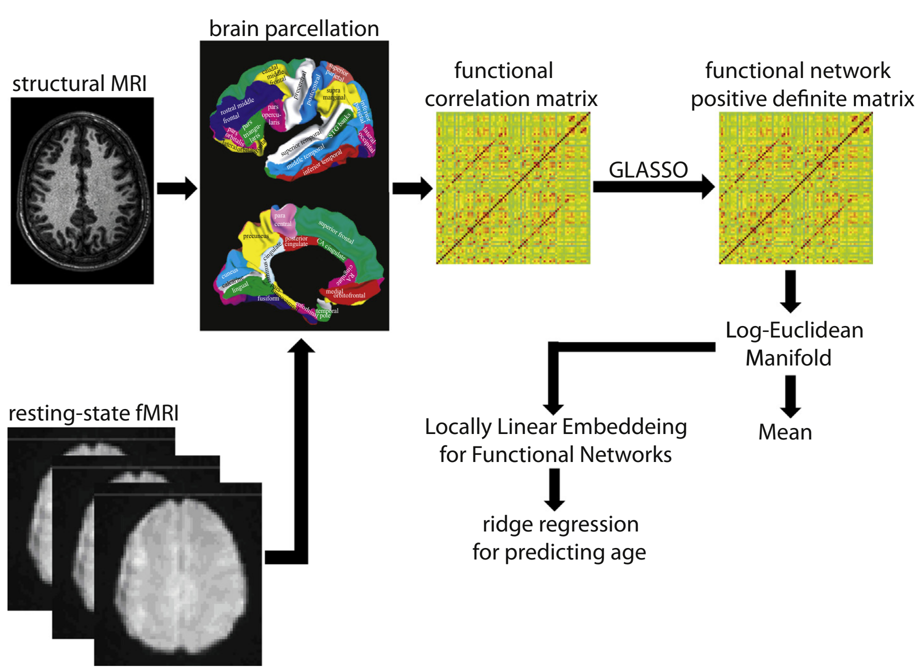

Fig. 2. Schematic of functional network analysis.

when the sample size of the data (e.g., time points in the resting state fMRI data) is substantially larger than the number of brain regions modeled, i.e., $n \gg p$. To resolve this singularity problem of the covariance matrix, the above log-likelihood can be regularized with **L**1-norm penalty. Hence, Eq. (1) can be extended as

$$L(R^{-1}) = \log\det R^{-1} - \mathrm{trace}(R^{-1}S) - \lambda\|R^{-1}\|_1, \tag{2}$$

where $\|\cdot\|_1$ is the sum of the absolute values of the elements of R^{-1}. $\lambda > 0$ controls the sparsity of the off-diagonal elements of R^{-1}. This penalized log-likelihood is maximized over the space of all possible symmetric positive definite (SPD) matrices. It has been shown that Eq. (2) is a convex problem and is usually solved using the graphical LASSO (GLASSO) algorithm (Ng et al., 2013; Banerjee et al., 2006, 2008; Friedman et al., 2008; Huang et al., 2010; Mazumder and Hastie, 2012).

2.4. Log-Euclidean Riemannian manifold of brain functional networks

Denote the functional networks as $R_i,\ i = 1, 2, \ldots, N$, where N is the number of subjects. It is important to compute the mean among them, denoted as $\bar{R}$, and study the variation of R_i deviated from $\bar{R}$ for understanding the representation of the functional network among the population and individual differences in functional connectivity. From the construction described in Section 2.3, R_i is a SPD matrix. Computing $\bar{R}$ is not trivial. For instance, the arithmetic mean of $R_i,\ i = 1, 2, \ldots, N$, where $\bar{R}$ does not satisfy certain desirable properties. The mean of $R_i^{-1},\ i = 1, 2, \ldots, N$ is not necessary to coincide with $\bar{R}^{-1}$. Moreover, any non-convex Euclidean operations on R_i could result in symmetric matrices with null or negative eigenvalues. As a consequence, there have been great efforts on carrying out computations with SPD matrices in a Riemannian manifold. In this study, we adopt the Log-Euclidean Riemannian structure on SPD matrices introduced by Arsigny et al. (2007) to compute the mean and interpolation of the functional networks because of its fast and efficient computation. It has been shown that there is a one-to-one and onto mapping between this SPD Riemannian space and a vector space of symmetric matrices. SPD matrices can be mapped to the vector space of symmetric matrices through the matrix logarithm operation, while symmetric matrices can be mapped to the SPD Riemannian space via the operation of the matrix exponential. Under this construction, SPD matrices are transformed into their matrix logarithms and the Riemannian computations can be converted into Euclidean ones for symmetric matrices. Hence, the distance between R_i and R_j can be computed via a Euclidean norm of symmetric matrices, that is,

$$dist(R_i, R_j) = \|\log(R_i) - \log(R_j)\|,$$

where $\|\cdot\|$ represents matrix norm. This distance is called as Log-Euclidean metric. In this work, we use the similarity-invariant Log-Euclidean metric, which is given by

$$\begin{aligned} dist(R_i, R_j) &= \|\log(R_i) - \log(R_j)\|_F \\ &= \left(\mathrm{trace}\{\log(R_i) - \log(R_j)\}^2\right)^{\frac{1}{2}}. \end{aligned} \tag{3}$$

$\|\cdot\|_F$ is the Frobenius norm of a matrix. With this metric, the SPD Riemannian space is *isomorphic* and *isometric* to the corresponding Euclidean space of symmetric matrices. Hence, one can easily compute the Frèchet mean of SPD matrices by minimizing

$$f(\bar{R}) = \sum_{i=1}^{N} dist(R_i, \bar{R})^2, \tag{4}$$

where

$$\bar{R} = \exp\left(\frac{1}{N}\sum_{i=1}^{N}\log(R_i)\right). \tag{5}$$

2.5. Locally linear embedding of brain functional networks

The functional organization of the brain is not random. We thus assume that variations of the functional networks are driven by variations in a small subset of unknown parameters. We present a nonlinear dimensionality reduction algorithm specifically for the purpose of approximating the SPD Riemannian space of the brain functional networks by a low-dimensional space where the relationship of neighborhood brain functional networks in the SPD Riemannian space can be preserved. We shall call this algorithm as Locally Linear Embedding-SPD (LLE-SPD) and it is an extension of the Locally Linear Embedding (LLE) algorithm (Tenenbaum et al., 2000; Roweis and Saul, 2000; Saul and Roweis, 2003), which assumes that the local neighborhood of a point on the manifold can be well approximated by the affine subspace spanned by the K-nearest neighbors (KNN) of the point and finds a low-dimensional embedding of the data based on these affine approximations. We make the assumption that the brain functional network of the ith subject and its neighbors (subjects whose metric distance to the ith subject is smaller than a certain threshold) to lie on or close to a locally linear patch of the low-dimensional manifold. Just as in LLE, we assume that every subject's brain functional network can be reconstructed from its K closest neighbors. While LLE has been applied to a variety of imaging problems, it uses (at least locally) the Euclidean metric or a variation of it to perform dimensionality reduction. While this may be appropriate in some cases, there are several problems where it is more natural to consider features that live in a non-Euclidean space. Goh and Vidal (2007, 2008) extends LLE to Riemannian manifolds, by making use of the Riemannian operations such as the exponential and logarithm maps. Yang et al. (2011) extends LLE to a diffeomorphic shape space for anatomical shape classification. Here, we employ the similar idea to reduce the dimensionality of the brain functional networks as those in Goh and Vidal (2007), Yang et al. (2011) and Tenenbaum et al. (2000). We will detail each step below.

The first step of LLE-SPD is the computation of the KNN associated with each functional network. Instead of using the Euclidean distance, we define the set of the ith subject's KNN, $\mathcal{N}_i$, as the K networks R_j that have the shortest metric distance to R_i computed based on Eq. (3). The second step of LLE-SPD is to find a matrix of weights $W \in \mathbb{R}^{N\times N}$, which characterize the each functional network as a linear combination of its neighbors. This is made possible by the linearity property of symmetric matrices. The coefficients W_{ij} can be estimated by minimizing reconstruction errors quantified in terms of the similarity-invariant Log-Euclidean metric as given in Eq. (3),

$$\epsilon(W) = \sum_{i=1}^{N}\|\log(R_i) - \sum_{j\in\mathcal{N}_i} W_{ij}\log(R_j)\|_F^2, \tag{6}$$

subject to $\sum_j W_{ij} = 1$ and $W_{ij} = 0$ when $j \notin \mathcal{N}_i$, and R_i is a SPD matrix representing the brain functional network. The coefficients W_{ij} summarize the contribution of the jth subject's functional network to that of the ith subject. Notice that the cost function becomes the same form of the cost function of the LLE algorithm first proposed in (Roweis and Saul, 2000) but in the vector space of symmetric matrices. Therefore, the optimal coefficients W_{ij} can be found by solving the least-squares problem given in (Roweis and Saul, 2000). More precisely, for each functional network R_i, the nonzero entries corresponding to the ith row of W are given by

$$W_i = \frac{\mathbf{1}^\top C_i^{-1}}{\mathbf{1}^\top C_i^{-1}\mathbf{1}}, \tag{7}$$

where $C_i \in \mathbb{R}^{K\times K}$ is the local Gram matrix at R_i, i.e., $C_i(j,l) = (R_j - R_i)^\top(R_l - R_i)$, and $\mathbf{1} \in \mathbb{R}^K$ is the vector of all ones. Just as in LLE and its extension for the Log-Euclidean Riemannian manifold, the weights W_{ij} in LLE-SPD reflect intrinsic geometric properties of the functional networks that are invariant to rotation, translation, and rescaling. Therefore, their characterization of local geometry in the original SPD Riemannian manifold is equally valid for that of the low-dimensional space. The last step of LLE-SPD is to find a low-dimensional representation of the data points. We assume that the same coefficients W_{ij} that reconstruct the ith subject functional network in the Log-Euclidean space can also be used to model its coordinates in the manifold with d dimensions. Assume that there is the mapping of R_i to a low-dimensional vector $\boldsymbol{y}_i$ such that $\boldsymbol{y}_i$ minimizes this embedding cost function

$$J([\boldsymbol{y}_1, \boldsymbol{y}_2, \ldots, \boldsymbol{y}_N]) = \sum_{i=1}^{N} \|\boldsymbol{y}_i - \sum_{j \in \mathcal{N}_i} W_{ij} \boldsymbol{y}_j\|^2, \tag{8}$$

subject to $\sum_{i=1}^{N} \boldsymbol{y}_i = 0, \frac{1}{N}\sum_{i=1}^{N} \boldsymbol{y}_i \boldsymbol{y}_i^\top = \mathtt{Id}_{N\times N}$, $\mathtt{Id}_{N\times N}$ is an $N \times N$ identity matrix. The two constraints ensure that the center of embedding is the origin, and $\boldsymbol{y}_i$ has a unit length. It has been proved (Roweis and Saul, 2000) that the embedding cost function is equivalent to

$$J(Y) = \text{trace}(Y^\top M Y),$$

where $Y = [\boldsymbol{y}_1, \boldsymbol{y}_2, \ldots, \boldsymbol{y}_N]$ and $M = (\mathtt{Id}_{N\times N} - W)^\top (\mathtt{Id}_{N\times N} - W)$. This can be solved through a sparse $N \times N$ eigenvalue problem whose bottom d nonzero eigenvectors of M provide an ordered set of orthogonal coordinates centered on the origin.

Note that there are two free parameters in the LLE-SPD algorithm which are the number of neighbors K and the intrinsic dimension of a set of functional networks d. In general, d is less than K. By nature, the LLE-SPD approach embeds the samples in the low-dimensional Euclidean space such that the relationship of the samples in the Riemannian manifold can be best preserved in the embedded Euclidean space. Hence, we optimize these two parameters via quantifying the similarity between the neighborhood relations in the Log-Euclidean Riemannian space of SPD and in the d-dimensional space at a fixed K and d, by $\boldsymbol{\rho}(D, D^K)$, where $\boldsymbol{\rho}(x, y)$ is the absolute correlation between variables x and y. D is the pair-wise metric distance matrix among R_i, while D^K is the pair-wise Euclidean distance matrix among the embeddings of R_i in the d-dimensional space when the K neighbors are used in LLE-SPD. We maximize $\boldsymbol{\rho}$ to determine the values of K and d using exhaustive search in this paper.

2.6. Explicit mapping of functional networks

In the previous section, we present how to use LLE-SPD to provide an embedding for a training set with N brain networks, $\{R_i\}_{i=1}^N$, to a d-dimensional space. For this, we adopted the procedure similar to that in Saul and Roweis (2003). If we are given a previously unseen functional network R_{N+1}, we want to compute a new embedding $\mathbf{y}_{N+1}$ that represents R_{N+1} in the d-dimensional space. It is obvious that one can incorporate R_{N+1} into the training set and find the low-dimensional embedding by running LLE-SPD on $\{R_i\}_{i=1}^{N+1}$. However, such a strategy is computationally costly when the training set is large scale. Therefore, an efficient algorithm is needed to derive an explicit mapping between the SPD Log-Euclidean space and the d-dimensional space obtained from the previous run of the LLE-SPD algorithm on $\{R_i\}_{i=1}^N$. In this section, we show how to extend LLE-SPD to a new data point R_{N+1}, without having to rerun LLE-SPD on the entire dataset. We introduce the following non-parametric solution to compute the low-dimensional embedding $\boldsymbol{y}_{N+1}$ for a new functional network R_{N+1}. We first calculate the metric distance between R_{N+1} and R_i, $i = 1, 2, \ldots, N$ and identify the KNN of R_{N+1} from R_i. Having obtained the KNN, it is then possible to find the coefficients $\widehat{W}_j$ and reconstruct $\boldsymbol{y}_{N+1}$ from $\widehat{W}_j$ and the existing embedding $\{\boldsymbol{y}_i\}_{i=1}^N$ by minimizing the reconstruction error given in Eq. (6). The low-dimensional embedding is given by $\boldsymbol{y}_{N+1} = \sum_{j \in \mathcal{N}_{N+1}} \widehat{W}_j \boldsymbol{y}_j$.

2.7. Prediction analysis

Ridge regression, which is sometimes known as linear least square regression with Tikhonov regularization, was used to predict biological age from the embedding of brain functional networks. Leave-one-out cross-validation was employed to estimate the prediction accuracy in age. We summarize the leave-one-out cross-validation procedure in Algorithm 1.

Algorithm 1. (Leave-one-out cross-validation)

1. compute the correlation matrix based on rs-fMRI time series data for each subject to construct matrix, S, in Eq. (2).
2. estimate a SPD matrix, R, from Eq. (2) using GLASSO algorithm. for $i = 1, \ldots, N$,
3. obtain the low-dimensional embedding of SPD matrices of $N-1$ subjects using LLE-SPD described in Section 2.5.
4. estimate the ridge regression model with the low-dimensional embedding data of $N-1$ subjects as independent variables and age as dependent variable. The parameter in the ridge regression model was 0.5 in our experiment.
5. project the SPD matrix of the Nth subject to the low-dimensional embedding using the explicit mapping described in Section 2.6.
6. predict the biological age of the Nth subject using ridge regression.

end.

3. Results and discussion

3.1. Prediction of biological age

In our experiment, we analyzed rs-fMRI data of 178 subjects by following the flow chart shown in Fig. 2. We first estimated the parameters, including the sparsity of the brain network in Eq. (2) and the neighbors and dimension in LLE-SPD, by maximizing the similarity between the neighborhood relations in the Log-Euclidean space of SPD and in the low-dimensional embedding space. The maximal similarity was achieved when the sparsity level of the brain network was 0.25, the number of neighbors in the LLE-SPD algorithm was 33, and the dimensionality for the LLE-SPD algorithm was 6. Fig. 3A shows the first three embedding dimensions of the brain functional networks. If the variation of brain functional networks is mainly because of age, we expect that the LLE-SPD algorithm is able to project the functional network into the dimension that is correlated with age. Indeed, the second row of Table 1 shows significant correlation of the first three embedded dimensions with age ($p < 0.001$). The ridge regression with the leave-one-out cross-validation was used to predict the biological age of each functional network. The predicted biological age was correlated with the subjects' actual age (Pearson correlation: $r = 0.591$, $p < 0.001$). The root mean square error (RMSE) between the two was 12.97.

In contrast, we applied the similar technique when considering the SPD is an element in the finite dimensional vector space where the norm of SPDs is the Frobenius norm of two SPDs. In this setting, the optimal embedding was achieved when the sparsity level of the brain network was 0.2. The number of neighbors in the LLE algorithm was 36, and the dimensionality of the LLE algorithm

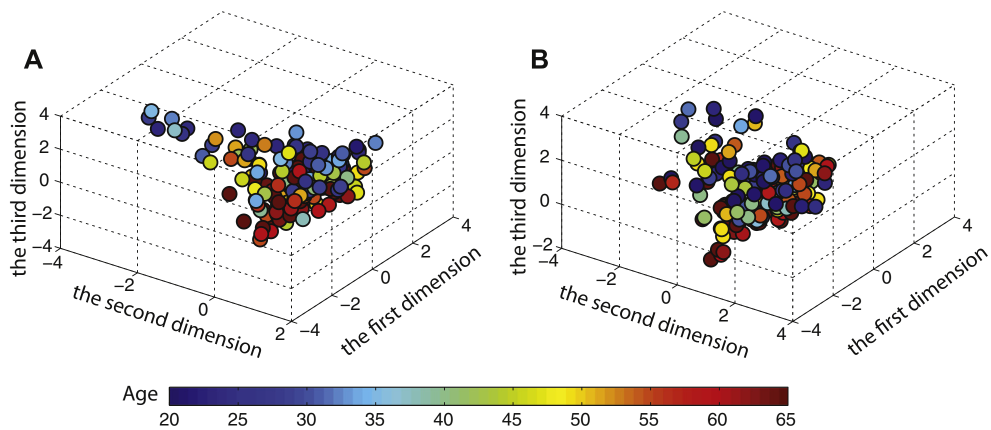

Fig. 3. The first three dimensions of embeddings of the brain functional networks. Panel (A) shows the embedding of the brain functional networks using LLE-SPD in the Log-Euclidean manifold space, while panel (B) illustrates the embedding of the brain functional networks using LLE in the Euclidean space.

Table 1
Correlation coefficients between age and the first three embedding dimensions of the brain functional networks. The second row lists the results obtained from locally linear embedding for symmetric positive definite matrices in the Log-Euclidean space (LLE-SPD). The third row lists the results obtained from locally linear embedding for symmetric positive definite matrices in the Euclidean space (LLE).

Pearson correlation r	1st	2nd	3rd
LLE-SPD	0.403 ($p < 0.001$)	0.308 ($p < 0.001$)	0.273 ($p < 0.001$)
LLE	0.380 ($p < 0.001$)	0.246 ($p < 0.001$)	0.218 ($p = 0.003$)

was 8. Fig. 3B shows the first three embedding dimensions of the brain functional networks obtained from LLE. The third row of Table 1 shows the correlation coefficients of these three dimensions with age. The predicted biological age was correlated with the subjects' actual age (Pearson correlation: $r = 0.457$, $p < 0.001$). The root mean square error (RMSE) between the two was 14.35.

Our results suggest that the Log-Euclidean manifold framework can provide more efficient and succinct representation of the functional network than the Euclidean framework does. This is indicated by a fewer dimension extracted by LLE-SPD in the Log-Euclidean manifold framework (6 dimensions in the Log-Euclidean framework vs 8 dimensions in the Euclidean framework). We further employed bootstrapping to estimate the empirical distribution of RMSE for both Log-Euclidean and Euclidean frameworks. Rank sum test showed that the integration of the Log-Euclidean manifold with LLE-SPD statistically significantly improved the age prediction when compared to the Euclidean framework ($p < 0.001$).

3.2. Evolution of brain functional networks across lifespan

We employed Eq. (5) and computed the SPD matrices averaged across subjects in each decade to represent the evolution of the brain function network across lifespan. The first column of Fig. 4 shows the mean of the brain functional networks among the 20- to 30-year olds, the 30- to 50-year olds, the 50- to 60-year olds, and the 60- to 79-year olds from the top to the bottom, respectively. For the purpose of visualization, we demonstrate the mean of the brain functional network in the sparse matrix form (see the second column of Fig. 4) and in the network graph (see the third and fourth columns of Fig. 4), where the sparse matrix was generated by first computing p-value of the correlation coefficients of functional signals between two brain regions and then controlling for multiple comparisons using False Discovery Rate (FDR). The mean of the functional network for 20- to 30-year olds is composed of six functional subnetworks, including visual, sensory, default mode network (DMN), salience, amygdala-hippocampus complex, and executive networks. The second column of Table 2 lists the structures in each of these functional subnetworks, which can also be visualized in Fig. 4A. For example, the sensory network consists of bilateral precentral, postcentral, and paracentral cortices as well as superior temporal and Heschl's gyri. Largely consistent with findings in previous studies (Buckner et al., 2008; Biswal et al., 2010; Damoiseaux et al., 2008b; Greicius et al., 2003), our study shows that DMN consists of bilateral precuneus, isthmuscingulate, middle temporal gyrus, inferior temporal and parietal cortices. The salience network is composed of the anterior cingulate, insular, posterior cingulate, basal ganglia, and thalamus. In particular, the anterior cingulate, insular, and thalamus have been identified as key structures of the salience network (Seeley et al., 2007). The mean of the functional network for the 30- to 50-year olds is similar to that seen for the 20s olds. However, the salience network is partially merging with the frontal structures in the executive network in the 20- to 30-year olds (see Fig. 4 A, B). Moreover, the temporal structures, such as superior, middle and inferior cortices, form a new temporal network in the 30- to 50-year olds (see Table 2). The mean of the functional network for the 50- to 60-year olds has the similar functional organization as that for the 30- to 50-year olds. However, the salience network only consists of the anterior and posterior cingulate as well as insular without involvement of subcortical structures and frontal structures. The functional reorganization was seen among the salience, executive, and emotional networks. Fig. 4C clearly shows reductions in functional connections across the whole brain as well as between subcortical and cortical regions. Fig. 4D shows less integration of the functional network in the 60- to 79-year olds, which is consistent with age-related reductions in global and local communication efficiencies in the brain (Bullmore and Sporns, 2012). Overall, the visual, sensory, and amygdala-hippocampus networks remain relatively stable in aging in terms of regional connections. Nevertheless, we observe the important evolution of functional networks across the lifespan. First, we observe the relatively stable organization of DMN based on the functional connections as precuneus, isthmuscingulate, and inferior parietal cortices are identified as the key structures in DMN across the lifespan. However, the strength of the DMN connectivity is reduced due to aging (see the first two columns of Fig. 4), which is in agreement with the findings shown in previous rs-fMRI studies (Damoiseaux et al., 2008a; Bluhm et al., 2008; Wang et al., 2010; Tomasi and Volkow, 2012). Second, our result suggests age-related functional disconnection between the subcortical and cortical structures,

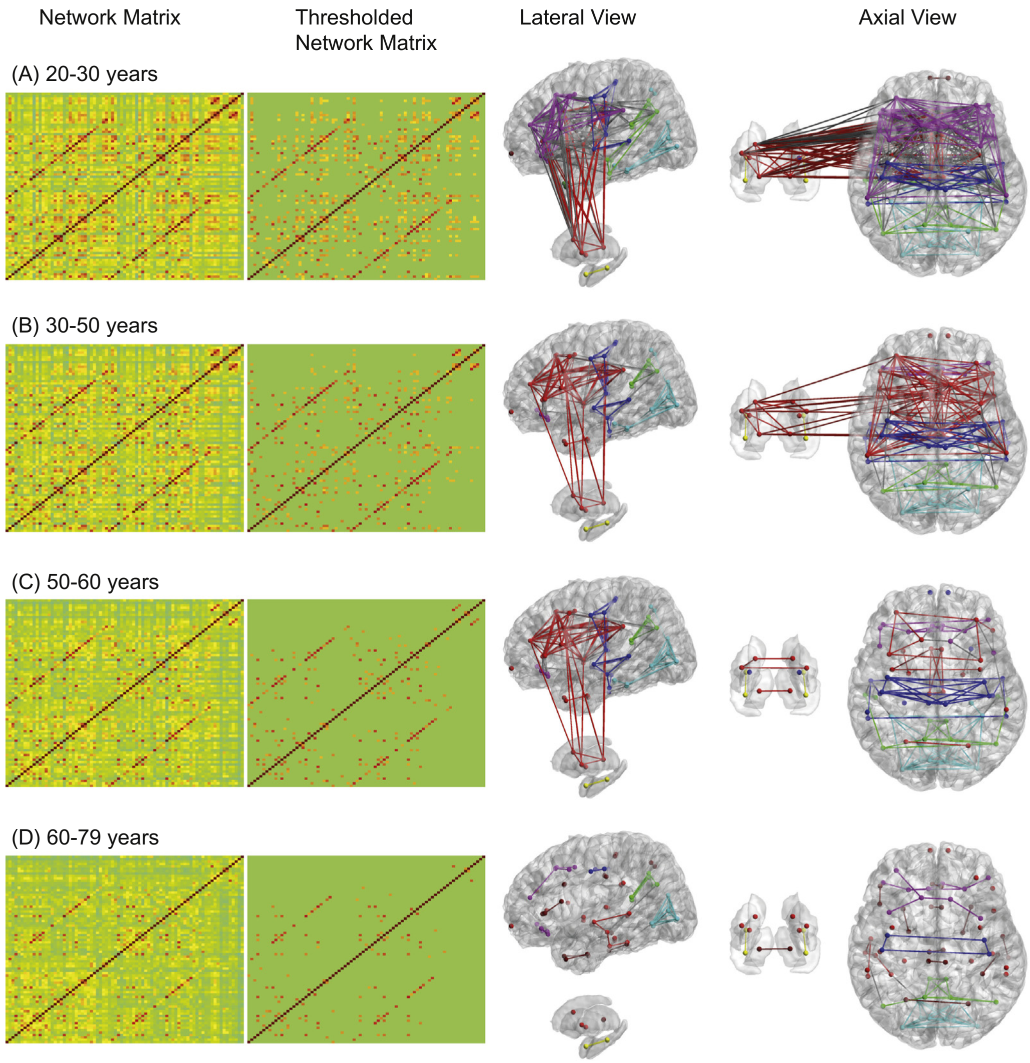

Fig. 4. Brain functional networks averaged in subjects at 20s (the first row), 30s and 40s (the second row), 50s (the third row), 60s and 70s years old (the fourth row). The first two columns show the average brain network in the matrix form without and with thresholding. The third and fourth columns show the average brain network in the graph mode. In the third column, the cortical surface is illustrated on the top panel and the subcortical surface is shown on the bottom panel. In the fourth column, the cortical surface is shown on the right panel and subcortical surface on the left panel.

especially disconnection between subcortical and frontal structures, which is in line with converging data from positron emission tomography (PET), diffusion tensor imaging (DTI), and neurocognition in aging. Garraux et al. (1999) show subcortical-frontal metabolic impairment in normal aging. Westlye et al. (2010) suggest age-related disruptions in major fiber bundles connecting subcortical and cortical structures. Ystad et al. (2011) employ DTI and rs-fMRI and show that unique cortico-subcortical fiber bundles can be identified for a range of cortical resting state networks, and indicate that these structural connections play an important role in subcortical–cortical resting state network communication. Hence, it is not surprising that pathways between the subcortical and cortical regions critically influence various aspects of cognition, motor control, and affect in aging (Bonelli and Cummings, 2007). Third, the salience, executive, and emotional networks are dynamically integrated and/or segregated across the lifespan. He et al. (2013) show that the connection of the salience network with the executive network and DMN is degraded even in middle-aged adults. Our study extends this result and shows that the insular is emerging with the dorsolateral prefrontal structures in 30- to 50-year olds, then separated in 50- to 60-olds, and finally emerging again in 60- to 79-year olds. This may influence the role of the salience in effectively switching between the executive network and DMN and may further affect cognitive function in aging population (Menon and Uddin, 2010).

4. Further consideration and limitations

Even though our paper only focused on the LLE manifold learning approach, other manifold learning approaches, such as ISOMAP and Laplacian Eigenmaps, can be employed for the purpose of the dimensionality reduction of the brain functional organization for the prediction of biological age. Nevertheless, the integration of LLE with the Log-Euclidean manifold of brain functional networks provides a natural framework where linear operations can be applied for the embedding and explicit mapping of the brain functional networks into a low-dimensional space. Therefore, this paper mainly extends the LLE algorithm to the Log-Euclidean manifold.

In addition to functional networks, our approach can also be applied to structural networks, such as structural networks derived from cortical thickness. More broadly, the Log-Euclidean Riemannian manifold and its associated metric provide easy and efficient computation of linear operations on SPD matrices. Hence, the presented framework can be easily incorporated with linear classifier for classification problems when SPD matrices are considered as features.

Table 2
Brain functional subnetworks across the lifespan.

Network	20–30 years	30–50 years	50–60 years	60–79 years
Visual	Cuneus	Cuneus	Cuneus	Cuneus
	Lingual	Lingual	Lingual	Lingual
	Lateral occipital cortex	Lateral occipital cortex	Lateral occipital cortex	Lateral occipital cortex
	Pericalcarine	Pericalcarine	Pericalcarine	Pericalcarine
	Fusiform	Fusiform	Fusiform	
	Parahippocampus	Parahippocampus	Parahippocampus	
		Entorhinal	Entorhinal	
		Temporal pole	Temporal pole	
		Globus pallidus	Globus pallidus	
Sensory	Precentral	Precentral	Precentral	Precentral
	Postcentral	Postcentral	Postcentral	Postcentral
	Paracentral	Paracentral	Paracentral	
	Superior temporal gyrus			
	Heschl's gyrus	Heschl's gyrus		
Default mode network	Precunes	Precunes	Precunes	Precunes
	Isthmuscingulate	Isthmuscingulate	Isthmuscingulate	Isthmuscingulate
	Middle temporal		Middle temporal	
	Inferior parietal	Inferior parietal	Inferior parietal	Inferior parietal
	Inferior temporal		Inferior temporal	
Salience and executive	Caudal anterior cingulate	Caudal anterior cingulate	Caudal anterior cingulate	
	Rostral anterior cingulate	Rostral anterior cingulate		
	Posterior cingulate	Posterior cingulate	Posterior cingulate	Posterior cingulate
	Insular	Insular	Insular	Insular
	Caudate	Caudate		Caudate
	Putamen	Putamen		Putamen
	Globus pallidus	Globus pallidus		Globus pallidus
	Thalamus	Thalamus		Thalamus
		Superior frontal		
		Caudal middle frontal		
		Rostral middle frontal		Rostral middle frontal
		Parsopercularis		Parsopercularis
		Parstriangularis		
				Frontal pole
				Supramaginal
				Parahippocampus
Amygdala-hippocampus	Amygdala	Amygdala	Amygdala	Amygdala
	Hippocampus	Hippocampus	Hippocampus	Hippocampus
Temporal		Superior temporal	Superior temporal	Superior temporal
		Middle temporal	Heschl's gyrus	Middle temporal
		Inferior temporal		Inferior temporal
Executive	Caudal middle frontal		Caudal middle frontal	Caudal middle frontal
	Rostral middle frontal		Rostral middle frontal	Rostral middle frontal
	Superior frontal		Superior frontal	Superior frontal
	Parsopercularis		Parsopercularis	
	Parsorbitalis	Parsorbitalis		
	Parstriangularis		Parstriangularis	
	Lateral orbitofrontal	Lateral orbitofrontal		
	Medial orbitofrontal	Medial orbitofrontal		
	Supramarginal		Supramarginal	
Emotion			Lateral orbitofrontal	Lateral orbitofrontal
			Medial orbitofrontal	Medial orbitofrontal
			Rostral anterior cingulate	
			Parsopercularis	
			Parsorbitalis	Parsorbitalis
			Parstriangularis	

Note. The structures that are not included in this table were not classified into any functional module.

We noticed that our study employed the cortical parcellation based on the gyral and sulcal pattern (Fischl et al., 2004). Even though the findings on the evolution of brain functional networks across lifespan are meaningful, the cortical parcellation based on brain functional units may improve the accuracy for predicting age. Nevertheless, the Log-Euclidean representation of the brain functional network can be employed for any cortical parcellation.

Acknowledgments

This study is supported by the Young Investigator Award at the National University of Singapore (NUSYIA FY10 P07), the National University of Singapore MOE AcRF Tier 1, and Singapore Ministry of Education Academic Research Fund Tier 2 (MOE2012-T2-2-130).

References

Achard, S., Bullmore, E., 2007. Efficiency and cost of economical brain functional networks. PLoS Comput. Biol. 3, e17.

Aljabar, P., Wolz, R., Srinivasan, L., Counsell, S., Rutherford, M., Edwards, A., Hajnal, J., Rueckert, D., 2011. A combined manifold learning analysis of shape and appearance to characterize neonatal brain development 30, 2072-2086. http://dx.doi.org/10.1109/TMI.2011.2162529.

Arsigny, V., Fillard, P., Pennec, X., Ayache, N., 2006. Log-Euclidean metrics for fast and simple calculus on diffusion tensors. Magnet. Reson. Med. 56, 411–421.

Arsigny, V., Fillard, P., Pennec, X., Ayache, N., 2007. Geometric means in a novel vector space structure on symmetric positive-definite matrices. SIAM J. Matrix Anal. Appl. 29, 328–347.
Banerjee, O., El Ghaoui, L., d'Aspremont, A., 2008. Model selection through sparse maximum likelihood estimation for multivariate Gaussian or binary data. J. Mach. Learn. Res. 9, 485–516.
Banerjee, O., Ghaoui, L., d'Aspremont, A., Natsoulis, G., 2006. Convex optimization techniques for fitting sparse Gaussian graphical models. In: Proceedings of the 23rd International Conference on Machine Learning, pp. 96.
Biswal, B., Mennes, M., Zuo, X., Gohel, S., Kelly, C., Smith, S., Beckmann, C., Adelstein, J., Buckner, R., Colcombe, S., Dogonowski, A., Ernst, M., Fair, D., Hampson, M., Hoptman, M., Hyde, J., Kiviniemi, V., Ktter, R., Li, S., Lin, C., Lowe, M., Mackay, C., Madden, D., Madsen, K., Margulies, D., Mayberg, H.S., McMahon, K., Monk, C., Mostofsky, S., Nagel, B., Pekar, J., Peltier, S., Petersen, S., Riedl, V., Rombouts, S., Rypma, B., Schlaggar, B., Schmidt, S., Seidler, R., Siegle, G., Sorg, C., Teng, G., Veijola, J., Villringer, A., Walter, M., Wang, L., Weng, X., Whitfield-Gabrieli, S., Williamson, P., Windischberger, C., Zang, Y., Zhang, H., Castellanos, F., Milham, M., 2010. Toward discovery science of human brain function. Proc. Natl. Acad. Sci. 107, 4734–4739.
Bluhm, R., Osuch, E., Lanius, R., Boksman, K., Neufeld, R., Theberge, J., Williamson, P., 2008. Default mode network connectivity: effects of age, sex, and analytic approach. Neuroreport 19, 887–891.
Bonelli, R.M., Cummings, J.L., 2007. Frontal-subcortical circuitry and behavior. Dialogues Clin. Neurosci. 9, 141–151.
Buckner, R., Andrews-Hanna, J., Schacter, D., 2008. The brain's default network: anatomy, function, and relevance to disease. Ann. NY Acad. Sci. 1124, 1–38.
Bullmore, E., Sporns, O., 2012. The economy of brain network organization. Nat. Rev. Neurosci. 13, 336–349.
Damoiseaux, J., Beckmann, C., Arigita, E., Barkhof, F., Scheltens, P., Stam, C., Smith, S., Rombouts, S., 2008a. Reduced resting-state brain activity in the default network in normal aging. Cereb. Cortex 18, 1856–1864.
Damoiseaux, J., Beckmann, C., Arigita, E., Barkhof, F., Scheltens, P., Stam, C., Smith, S., Rombouts, S., 2008b. Reduced resting-state brain activity in the default network in normal aging. Cereb. Cortex 18, 1856–1864.
Deligianni, F., Varoquaux, G., Thirion, B., Robinson, E., Sharp, D., Edwards, A., Rueckert, D., 2011. A probabilistic framework to infer brain functional connectivity from anatomical connections. In: Information Processing in Medical Imaging.
Dosenbach, N., Nardos, B., Cohen, A., Fair, D., Power, J., Church, J., Nelson, S., Wig, G., Vogel, A., Lessov-Schlaggar, C., Barnes, K., Dubis, J., Feczko, E., Coalson, R., Pruett, J.J., Barch, D., Petersen, S., Schlaggar, B., 2010. Prediction of individual brain maturity using fMRI. Science 329, 1358–1361.
Fillard, P., Pennec, X., Arsigny, V., Ayache, N., 2007. Clinical DT-MRI estimation, smoothing and fiber tracking with log-Euclidean metrics. IEEE Trans. Med. Imag. 26, 1472–1482.
Fischl, B., van der Kouwe, A., Destrieux, C., Halgren, E., Segonne, F., Salat, D.H., Busa, E., Seidman, L.J., Goldstein, J., Kennedy, D., Caviness, V., Makris, N., Rosen, B., Dale, A.M., 2004. Automatically parcellating the human cerebral cortex. Cereb. Cortex 14, 11–22.
Fischl, B., Salat, D.H., Busa, E., Albert, M., Dieterich, M., Haselgrove, C., van der Kouwe, A., Killiany, R., Kennedy, D., Klaveness, S., Montillo, A., Makris, N., Rosen, B., Dale, A.M., 2002. Whole brain segmentation: automated labeling of neuroanatomical structures in the human brain. Neuron 33, 341–355.
Friedman, J., Hastie, T., Tibshirani, R., 2008. Sparse inverse covariance estimation with the graphical lasso. Biostatistics 9, 432.
Garraux, G., Salmon, E., Degueldre, C., Lemaire, C., Laureys, S., Franck, G., 1999. Comparison of impaired subcortico-frontal metabolic networks in normal aging, subcortico-frontal dementia, and cortical frontal dementia. Neuroimage 10, 149–162.
Goh, A., Vidal, R., 2007. Segmenting motions of different types by unsupervised manifold clustering. In: IEEE Conference on Computer Vision and Pattern Recognition, pp. 1–6.
Goh, A., Vidal, R., 2008. Clustering and dimensionality reduction on Riemannian manifolds, in: IEEE Conference on Computer Vision and Pattern Recognition, pp. 1–8.
Greicius, M., Krasnow, B., Reiss, A., Menon, V., 2003. Functional connectivity in the resting brain: a network analysis of the default mode hypothesis. Proc. Natl. Acad. Sci. 100, 253–258.
He, X., Qin, W., Liu, Y., Zhang, X., Duan, Y., Song, J., Li, K., Jiang, T., Yu, C., 2013. Age-related decrease in functional connectivity of the right fronto-insular cortex with the central executive and default-mode networks in adults from young to middle age. Neurosci. Lett. 544, 74–79.
He, X., Yan, S., Hu, Y., Niyogi, P., Zhang, H., 2005. Face recognition using Laplacian faces. IEEE Trans. Pattern Anal. Mach. Intell. 27, 328–340.
Huang, S., Li, J., Sun, L., Ye, J., Fleisher, A., Wu, T., Chen, K., Reiman, E., 2010. Learning brain connectivity of Alzheimer's disease by sparse inverse covariance estimation. NeuroImage 50, 935–949.
Mazumder, R., Hastie, T., 2012. Exact covariance thresholding into connected components for large-scale graphical lasso. J. Mach. Learn. Res. 13, 781–794.
Menon, V., Uddin, L., 2010. Saliency, switching, attention and control: a network model of insula function. Brain Struct. Funct. 214, 655–667.
Meunier, D., Achard, S., Morcom, A., Bullmore, E., 2009. Age-related changes in modular organization of human brain functional networks. NeuroImage 44, 715–723.
Ng, B., Varoquaux, G., Poline, J.B., Thirion, B., 2013. A novel sparse group Gaussian graphical model for functional connectivity estimation. In: Information Processing in Medical Imaging, Asilomar, États-Unis. <http://hal.inria.fr/hal-00842607>.
Ng, T., Niti, M., Chiam, P., Kua, E., 2007. Ethnic and educational differences in cognitive test performance on mini-mental state examination in asians. Am. J. Geriatr. Psych. 15, 130–139.
Onoda, K., Ishihara, M., Yamaguchi, S., 2012. Decreased functional connectivity by aging is associated with cognitive decline. J. Cogn. Neurosci. 24, 2186–2198.
Pennec, X., Fillard, P., Ayache, N., 2006. A Riemannian framework for tensor computing. Int. J. Comput. Vis. 66, 41–66 (A preliminary version appeared as INRIA Research Report 5255, July 2004).
Qiu, A., Rosenau, B.J., Greenberg, A.S., Hurdal, M.K., Barta, P., Yantis, S., Miller, M.I., 2006. Estimating linear cortical magnification in human primary visual cortex via dynamic programming. NeuroImage 30, 999.
Roweis, S.T., Saul, L.K., 2000. Nonlinear dimensionality reduction by locally linear embedding. Science 290, 2323–2326.
Saul, L.K., Roweis, S.T., 2003. Think globally, fit locally: unsupervised learning of low dimensional manifolds. J. Mach. Learn. Res. 4, 119–155.
Seeley, W., Menon, V., Schatzberg, A., Keller, J., Glover, G., Kenna, H., Reiss, A., Greicius, M., 2007. Dissociable intrinsic connectivity networks for salience processing and executive control. J. Neurosci. 27, 2349–2356.
Tenenbaum, J.B., de Silva, V., Langford, J.C., 2000. A global geometric framework for nonlinear dimensionality reduction. Science 290, 2319–2323.
Tomasi, D., Volkow, N., 2012. Aging and functional brain networks. Mol. Psychiat. 17, 549–558.
Varoquaux, G., Baronnet, F., Kleinschmidt, A., Fillard, P., Thirion, B., 2010. Detection of brain functional-connectivity difference in post-stroke patients using group-level covariance modeling. In: Jiang, T., Navab, N., Pluim, J.P.W., Viergever, M.A. (Eds.), MICCAI. Springer, pp. 200–208.
Venkataraman, A., Kubicki, M., Golland, P., 2013. From brain connectivity models to region labels: Identifying foci of a neurological disorder. IEEE Trans. Med. Imag. 32, 2078–2098.
Wang, L., Laviolette, P., O'Keefe, K., Putcha, D., Bakkour, A., Van Dijk, K., Pihlajamki, M., Dickerson, B., Sperling, R., 2010. Intrinsic connectivity between the hippocampus and posteromedial cortex predicts memory performance in cognitively intact older individuals. NeuroImage 51, 910–917.
Wang, L., Su, L., Shen, H., Hu, D., 2012. Decoding lifespan changes of the human brain using resting-state functional connectivity MRI. PLoS One 7, e44530.
Westlye, L., Walhovd, K., Dale, A., Bjrnerud, A., Due-Tnnessen, P., Engvig, A., Grydeland, H., Tamnes, C., Ostby, Y., Fjell, A., 2010. Life-span changes of the human brain white matter: diffusion tensor imaging (DTI) and volumetry. Cereb. Cortex 20, 2055–2068.
Wu, T., Zang, Y., Wang, L., Long, X., Hallett, M., Chen, Y., Li, K., Chan, P., 2007. Aging influence on functional connectivity of the motor network in the resting state. Neurosci. Lett. 422, 164–168.
Yang, X., Goh, A., Qiu, A., 2011. Locally linear diffeomorphic metric embedding (LLDME) for surface-based anatomical shape modeling. NeuroImage 56, 149–161.
Ystad, M., Hodneland, E., Adolfsdottir, S., Haasz, J., Lundervold, A., Eichele, T., Lundervold, A., 2011. Cortico-striatal connectivity and cognition in normal aging: a combined DTI and resting state fMRI study. Neuroimage 55, 24–31.